Crimson Publishers
Wings to the Research

Research Article

Nickel and Cobalt-Doped Cerium Dioxide Nanohybrids for Efficient Photo-Degradation of Methylene Blue Dye

Haider Ali[1], Maqbool Hussain[1]*, Gulam Ali[2] and Shafqat Munir[3]

[1]Department of Physics, University of Agriculture, Pakistan

[2]Department of Computer Science, University of Okara, Pakistan

[3]Department of Chemistry, Minhaj University, Pakistan

ISSN: 2770-6745

***Corresponding author:** Maqbool Hussain, Department of Physics, University of Agriculture, Faisalabad, Pakistan

Submission: December 8, 2025
Published: May 25, 2026

Volume 6 - Issue 1

How to cite this article: Haider Ali, Maqbool Hussain*, Gulam Ali and Shafqat Munir. Nickel and Cobalt-Doped Cerium Dioxide Nanohybrids for Efficient Photo-Degradation of Methylene Blue Dye. Biodiversity Online J. 6(1). BOJ. 000628. 2026.
DOI: 10.31031/BOJ.2026.06.000628

Abstract

The persistent pollution of textile wastewater by toxic azo dyes necessitates the development of efficient photocatalysts for solar-driven environmental remediation. In this study, cerium oxide (CeO_2) nanohybrids were individually doped with nickel (Ni) and cobalt (Co) via a facile sol-gel method to overcome the inherent UV-light dependency of the pristine material. Ni- and Co-doped CeO_2 nanoparticles were synthesized using precursor molar ratios of 1:150 and 1:50, respectively. Comprehensive characterization confirmed the successful incorporation of Ni and Co into the CeO_2 fluorite cubic lattice without the formation of secondary phases. Structural analysis revealed a uniform, spherical morphology with an average particle size of approximately 15nm. Crucially, the introduction of dopants enhanced the absorption of visible light. The photocatalytic efficiency of the nanohybrids was evaluated for the degradation of methylene blue under simulated solar irradiation, where both doped catalysts significantly outperformed their undoped counterpart. The Co-doped CeO_2 (1:50) achieved 96% degradation within 10 minutes, exhibiting a rate constant approximately 4.3 times higher than pristine CeO_2 under identical conditions. This enhanced activity is attributed to the dopant's role in creating abundant oxygen vacancies, which act as charge separation centres to suppress the recombination of photogenerated electron-hole pairs effectively. This work highlights that strategic doping of CeO_2 with transition metals is a powerful approach for engineering robust nanomaterials for solar-powered water purification.

Keywords: Cerium dioxide; Doping; Dye degradation; Sol-gel; Photocatalytic degradation

Introduction

The rapid pace of industrialization, while essential for economic growth, has led to significant environmental degradation, posing serious risks to ecosystems and human health [1]. A major contributor to this problem is the textile industry, which releases large volumes of wastewater containing synthetic organic dyes. Azo dyes, in particular, are a prominent class of pollutants known for their complex aromatic structures, high stability and resistance to biodegradation. Their presence in water bodies is a critical concern, as many of these compounds are carcinogenic, mutagenic and can cause a range of health issues from skin irritations to organ damage [1]. Consequently, the development of efficient and sustainable methods for the complete mineralization of these recalcitrant pollutants is a pressing global challenge. Among various wastewater treatment technologies, Advanced Oxidation Processes (AOPs) particularly heterogeneous photocatalysis, have emerged as a highly promising green solution [2,3].

This technique utilizes semiconductor materials to harness light energy, ideally from the sun, to generate highly reactive oxygen species that can non-selectively break down complex organic molecules into benign products like CO_2, H_2O, and mineral acids [4]. Cerium oxide (CeO_2), a rare earth metal oxide, has garnered significant attention as a potent photocatalyst

due to its abundance, low cost, non-toxicity and remarkable physicochemical properties. Its unique oxygen storage capacity and the facile Ce^{3+}/Ce^{4+} redox couple are particularly advantageous, as they promote charge transfer and the formation of surface oxygen vacancies, which are crucial for enhancing catalytic reactions [5]. Despite these promising attributes, the practical application of pristine CeO_2 in solar-driven processes is severely limited by its intrinsic wide band gap of approximately 3.6 eV. This property restricts its photo-activity almost exclusively to the ultraviolet (UV) portion of the solar spectrum, which constitutes only about 5% of the total solar irradiance, leaving the vast visible light region (~45%) largely unutilized [4,6]. To overcome this fundamental limitation and engineer a more efficient solar catalyst, modifying the electronic structure of CeO_2 is essential. Doping the host lattice with foreign atoms or ions has been established as a powerful strategy to manipulate the electronic, optical, and magnetic properties of nanostructures, often leading to a narrowed band gap and enhanced visible light absorption [7].

The incorporation of transition metals like nickel (Ni) and cobalt (Co) into oxide lattices is an effective method for tuning their photocatalytic properties [8]. These dopants can introduce new energy levels within the band gap of CeO_2, create additional oxygen vacancies to act as charge-trapping sites and ultimately suppress the rapid recombination of photogenerated electron-hole pairs, thereby improving the overall quantum efficiency. While single-metal doping has been widely explored, co-doping with multiple elements can introduce synergistic effects that lead to superior performance enhancements not achievable with individual dopants. A significant amount of research has been dedicated to elevating the effectiveness of photocatalysts through strategies like doping and the creation of semiconductor composites [9-11]. For instance, studies on cerium oxide (CeO_2) have demonstrated the positive impact of this approach. It has been shown that incorporating iron (Fe) into CeO_2 films leads to a marked improvement in their photocatalytic capabilities compared to pure, undoped films [10]. This enhanced performance was primarily attributed to a combination of a reduced band gap energy and an increased specific surface area. In a similar vein, other research has revealed that doping CeO_2 nanorods with cobalt (Co) results in excellent photocatalytic activity when the material is exposed to ultraviolet (UV) light [11]. Similarly, Ag-doped CeO_2 nanoparticles synthesized via the sol-gel method exhibited improved photocatalytic degradation of azo dyes under direct sunlight compared with pure CeO_2, which was attributed to enhanced optical properties, improved charge separation and uniform nanoparticle distribution [12]. The present study utilizes nickel (Ni) and cobalt (Co) as dopants within a cerium oxide (CeO_2) matrix. The central hypothesis is that the resulting doped nanostructures will exhibit a significant enhancement in their photocatalytic activity.

This study, therefore, focuses on the synthesis and characterization of novel Ni and Co-doped CeO2 nanohybrids designed for enhanced visible-light-driven photocatalysis. We aim to systematically investigate the structural, morphological and optical properties of the co-doped nanohybrid and evaluate its photocatalytic efficiency for the degradation of selected azo dyes under simulated solar irradiation. By elucidating the synergistic effects of Ni and Co doping, this work seeks to provide a rational design strategy for developing robust and highly efficient photocatalysts for environmental remediation.

Materials and Methods

Cerium (III) nitrate hexahydrate (Ce $(NO_3)_3 \cdot 6H_2O$, 99.5%), Nickel (II) nitrate hexahydrate (Ni $(NO_3)_2 \cdot 6H_2O$), Cobalt (II) nitrate hexahydrate (Co $(NO_3)_2 \cdot 6H_2O$), ammonium hydroxide (NH_4OH, 28-30% solution), urea (CH4N2O), hydrochloric acid (HCl, 37%), sodium hydroxide (NaOH), and methylene blue were purchased from Sigma-Aldrich (via Chem-Tech, Pakistan). All chemicals were of analytical grade and were used as received without further purification. Deionized (DI) water was used for the preparation of all aqueous solutions and for all washing steps throughout the experiments.

Synthesis of nano catalysts

Synthesis of cerium dioxide (CeO_2) nanoparticles: Cerium dioxide (CeO_2) nanoparticles were synthesized via a Sol-gel method, followed by a calcination step [13]. The procedure consisted of two main stages: the preparation of a stable CeO_2 nano-sol and its subsequent conversion to a nano powder. In a typical synthesis, a cerium precursor solution was prepared by dissolving 17.3g of cerium (III) nitrate hexahydrate in 200mL of DI water in a beaker under constant magnetic stirring. To this solution, ammonium hydroxide (28-30%) was added dropwise until the pH reached 11, resulting in the formation of a milky precipitate. The resulting precipitate was thoroughly washed three to four times with DI water to remove residual ions. The washing was performed by repeated cycles of centrifugation, decantation of the supernatant, and redispersion of the precipitate in fresh DI water. Separately, a urea solution was prepared by dissolving 2.4g of urea in 400mL of DI water. The pH of this solution was adjusted to 3 by the dropwise addition of hydrochloric acid (37%), and the solution was stirred for 30 minutes. The acidic urea solution was then added dropwise from a burette into the washed cerium precursor suspension under vigorous stirring. The resulting mixture was stirred for an additional hour to ensure homogeneity, yielding a stable cerium dioxide nano-sol. The final sol was stored in a refrigerator at 4 °C for further use and characterization.

Preparation of CeO_2 nano powder: To obtain the powder form, a 50mL aliquot of the as-prepared CeO_2 nano-sol was transferred to a ceramic crucible. The sol was dried in an oven at 65 °C for 40 hours, which resulted in the formation of a crystalline xerogel. The dried material was then ground into a fine powder using an agate mortar and pestle. Finally, the powder was calcined in a muffle furnace at 600 °C for 2 hours to obtain the crystalline CeO_2 nano powder. For the synthesis of doped CeO_2 nanoparticles, appropriate amounts of $Ni(NO_3)_2 \cdot 6H_2O$ and $Co(NO_3)_2 \cdot 6H_2O$ were added to the precursor solution to obtain molar ratios of 1:150 and 1:50, respectively, followed by continuous stirring (6 hours) and calcination under identical conditions as pristine CeO_2.

Characterization

The crystal structure and phase purity were analysed using X-ray diffraction (XRD) with Cu Kα radiation (λ =0.15406nm). The

surface morphology and elemental composition were examined using Scanning Electron Microscopy (SEM) coupled with Energy Dispersive X-ray (EDX) analysis. Chemical bonds and functional groups were identified using Fourier Transform Infrared (FTIR) spectroscopy over a range of 500-4000 cm^{-1}. The optical properties were determined using a UV-Visible spectrophotometer.

Photocatalytic activity measurement: The photocatalytic performance was evaluated by monitoring the degradation of Methylene Blue (MB) dye under simulated solar irradiation. In a typical experiment, 2mg of catalyst was dispersed in 100mL of dye solution. The suspension was first stirred in the dark for 30 minutes to establish adsorption-desorption equilibrium. Photocatalytic performance was evaluated for Methylene Blue (MB) degradation under simulated solar irradiation (92mW cm^{-2}). After centrifugation to remove the catalyst, the concentration of MB was determined by measuring its characteristic absorbance peak (~664nm) using a UV-Visible spectrophotometer. The degradation efficiency was calculated using the formula:

$$Degradation(\%) = [(C_o - C_t / C_o] \times 100$$

where C_o is the initial concentration, and C_t is the concentration at time t. The effects of catalyst dosage, initial dye concentration, and pH were systematically investigated to determine the optimal reaction conditions.

Results and Discussion

Structural and crystallographic analysis (XRD)

The crystal structure of the synthesized pure CeO_2, Ni-doped CeO2, and Co-doped CeO2 nanoparticles was investigated using XRD. As shown in Figure 1, all samples exhibit diffraction peaks at 2θ values of approximately 28.7°, 33.2°, 47.6°, 56.5°, and 59.2°. These peaks correspond to the (111), (200), (220), (311) and (222) crystal planes of the Face-Cantered Cubic (FCC) fluorite structure of CeO_2 (JCPDS card No. 43-1002). No diffraction peaks corresponding to impurity phases, such as nickel or cobalt oxides, were detected, confirming that Ni^{2+} and Co^{2+} ions were successfully incorporated into the CeO_2 host lattice. The broad nature of the peaks indicates the nanocrystalline character of the materials.

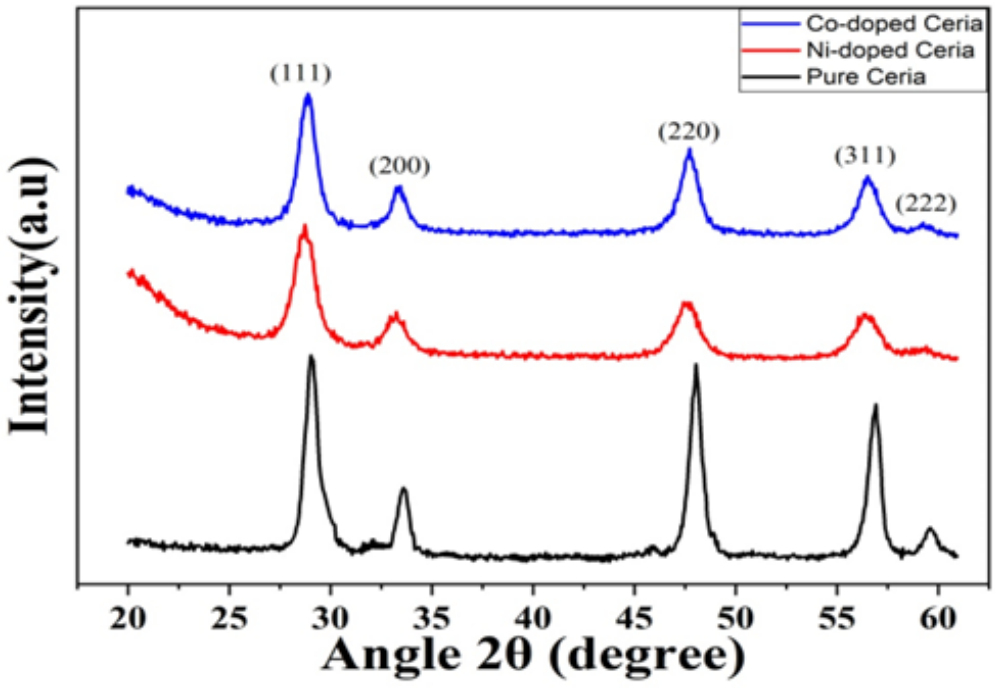

Figure 1: XRD patterns of undoped and Ni, Co-doped CeO2 nanostructures.

The average crystallite size (D) of the nanoparticles was calculated from the Full Width at Half Maximum (FWHM) of the most intense (111) diffraction peak using the Debye-Scherrer equation [14,15]:

$$D = \frac{k\lambda}{\beta \cos\theta}$$

where K is the Scherrer constant (0.9), λ is the wavelength of the Cu Kα radiation (0.15406nm), β is the FWHM in radians and θ is the Bragg angle. The calculated structural parameters are summarized in Table 1. The average crystallite size for pure CeO_2 was calculated to be 17.6nm. Upon doping, the crystallite size was slightly larger for Ni-doped CeO_2 (19.5nm) and slightly smaller for Co-doped CeO_2 (16.8nm). This variation is likely due to the lattice strain induced by the substitution of Ce4+ ions (ionic radius ~0.097nm) with dopant ions of different radii (Ni2+ ~0.069nm; Co^{2+} ~0.074nm). The small crystallite sizes obtained in this study can be attributed to the sol-gel synthesis method and the relatively low calcination temperature of 600 °C, which prevents excessive grain growth, consistent with previous reports (Aazam et al. 2011).

Table 1: Structural parameters derived from XRD data for pure and doped CeO_2 nanoparticles.

Sample	(HKL)	2θ (deg)	FWMH (rad)	Crystallite Size (nm)
Pure CeO_2	-111	28.7	0.0085	17.6
Ni-doped CeO_2	-111	28.7	0.0077	19.5
Co-doped CeO_2	-111	28.7	0.0076	16.8

Morphological and elemental analysis (SEM-EDX)

The surface morphology and particle size distribution of the undoped, Co-doped and Ni-doped CeO_2 nanoparticles were examined using Scanning Electron Microscopy (SEM), with representative micrographs presented in Figure 2. The SEM image of undoped CeO_2 (Figure 2a) reveals irregularly distributed spherical nanoparticles with noticeable agglomeration, forming larger secondary clusters, which is commonly observed in nanomaterials synthesized through wet-chemical methods due to their high surface energy. The particle surfaces appear relatively rough, consistent with nucleation and growth during the sol-gel process. The Co-doped CeO_2 sample (Figure 2b) also exhibits a predominantly spherical morphology with comparatively improved particle distribution. Rather than attributing this behaviour solely to reduced agglomeration, the incorporation of Co ions into the CeO_2 lattice may contribute to defect generation, lattice distortion and modified surface characteristics, which can influence charge-transfer properties and photocatalytic activity. The overall morphology confirms that doping did not significantly alter the fundamental nanostructure of CeO_2. The effect of doping is even more pronounced in the Ni-doped CeO_2 sample (Figures 2c&2d). These micrographs reveal more distinct and uniformly distributed spherical particles with a marked reduction in agglomeration. The particles appear to be more regular in shape and size, indicating that the presence of Ni^{2+} ions likely acts as a crystal growth inhibitor or morphology-directing agent during the synthesis. This controlled growth results in finer, more separated primary particles, which is consistent with findings where dopants are used to tune the nanostructure of metal oxides [16].

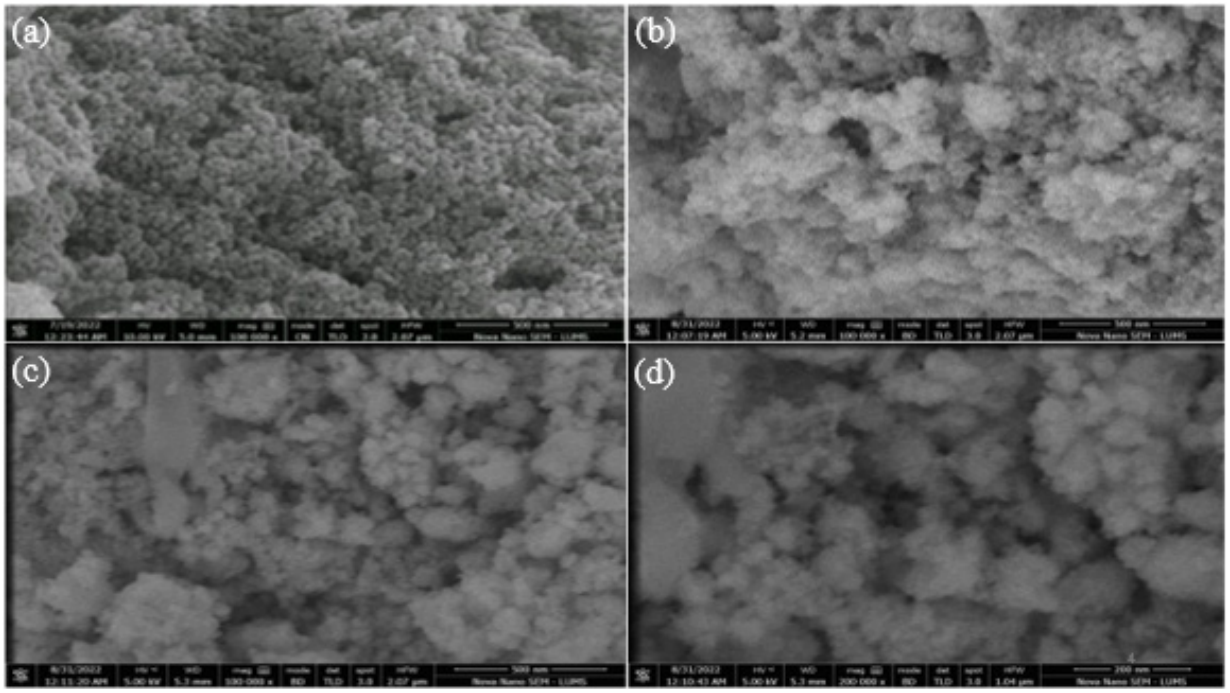

Figure 2: (a) SEM image of undoped CeO_2 nanostructures, (b) Co-CeO_2 and (c, d) Ni-CeO_2.

In summary, the SEM analysis confirms that while all synthesized materials are composed of nanoscale, spherical particles, doping with both Co and Ni effectively mitigates the agglomeration observed in pure CeO2. The improved dispersion and more uniform particle morphology in the doped samples are critical features, as they are expected to yield a higher accessible surface area and a greater density of active sites. These morphological advantages are anticipated to be directly responsible for enhanced photocatalytic performance.

Energy Dispersive X-ray (EDX) analysis was performed to confirm the elemental composition of the doped samples (Figure 3). The EDX spectrum for Co-doped CeO_2 (Figure 3a) confirms the presence of Cerium (Ce), Oxygen (O), and Cobalt (Co), verifying the successful incorporation of cobalt. Similarly, the spectrum for Ni-doped CeO_2 (Figure 3b) shows prominent peaks for Ce, O and Nickel (Ni). The detection of trace amounts of C, Si, Na, and Cl is likely attributable to precursors, handling, or the sample holder. The elemental mapping confirmed a uniform distribution of the dopant elements within the CeO_2 matrix.

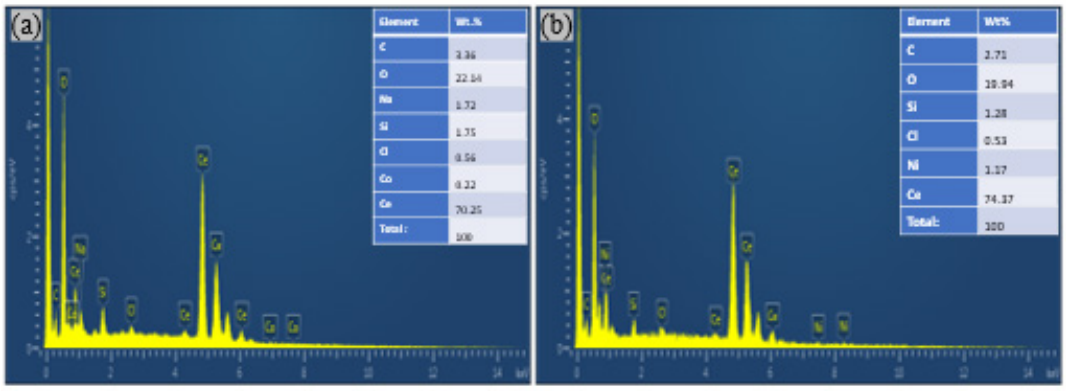

Figure 3: EDX Spectra and Elemental Mapping of (a) Co-doped CeO_2 (b) Ni-doped CeO_2 Nanoparticles.

Fourier transformation infrared radiation (FTIR)

Fourier Transform Infrared (FTIR) spectroscopy was employed to identify the chemical bonds and functional groups present in the synthesized materials [17,18]. The FTIR spectra for pure, Co-doped and Ni-doped CeO_2, recorded in the range of 500-4000cm^{-1}, are displayed in Figure 4. The spectra of all samples are dominated by two main features. A strong, broad absorption band cantered around 3430cm^{-1} and a weaker peak near 1700cm^{-1} are assigned to the O-H stretching and H-O-H bending vibrations of physically adsorbed water molecules on the surface of the nanoparticles. The most significant feature is the intense absorption peak observed below 700cm^{-1} (cantered around 700cm^{-1}), which is the characteristic vibrational mode of the Ce-O metal-oxygen bond in the fluorite lattice of CeO_2 [19]. The presence of this peak confirms the formation of the cerium dioxide framework. The similarity of the spectra across all samples further indicates that doping did not introduce new chemical bonds or significantly alter the fundamental structure of CeO_2.

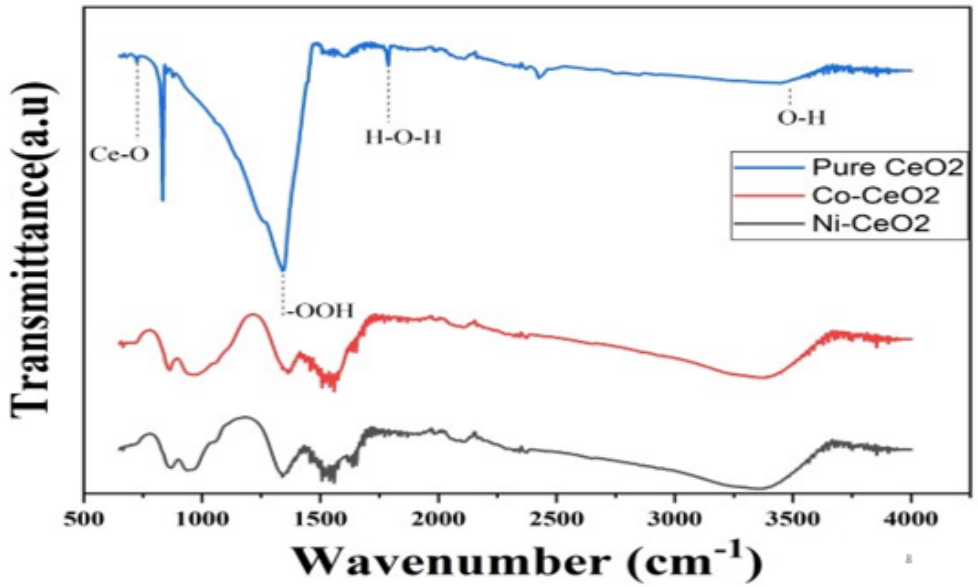

Figure 4: FT-IR spectra of undoped and Ni and Co-doped CeO_2 nanostructures.

Photocatalytic performance

The photocatalytic performance of nickel (Ni) and cobalt (Co) doped ceria (CeO^2) nanocomposites for the degradation of Methylene Blue (MB) was systematically evaluated. The Co-doped CeO_2 at a 1:50 ratio was identified as the superior catalyst, achieving complete dye degradation in a remarkable 8 minutes, significantly outperforming the optimal Ni-doped CeO_2 (1:150 ratio), which required 19 minutes. The study of reaction parameters revealed that the process is highly pH-dependent, with maximum efficiency observed at an alkaline pH of 11, which is attributed to the enhanced electrostatic attraction between the negatively charged catalyst surface and the cationic dye molecules. Furthermore, the catalyst's activity was found to be most effective at lower dye concentrations, as demonstrated by the rapid degradation of a 10 ppm MB solution. The absorption of the dye molecule is gradually reduced with intensifying irradiation time of degradation due to the deprivation of chromophore to form a transitional product. The degradation efficiency was calculated by

$$Degradation\% = \left\{ \frac{C_o - C}{C_o} \right\} \times 100$$

where C_0 and C are the initial and final concentrations of aqueous dye solution (10ppm). The degradation study was carried out with different catalysts, such as Ni-CeO_2 and Co-CeO_2.

The influence of catalyst dosage on photocatalytic efficiency was investigated for the optimized 1:150 Ni-CeO_2 and 1:50 cobalt-doped CeO_2 nanocomposites, with the degradation of a 10ppm Methylene Blue solution monitored over 20 and 10 minutes, respectively, at a constant pH of 11 (Figure 3a and 3b). The results demonstrate a clear dependence of the degradation rate on the amount of catalyst used. Initially, increasing the catalyst dosage enhances dye degradation due to the greater number of available active sites on the catalyst surface, which accelerates the generation of reactive oxygen species. However, beyond an optimal dosage, the degradation efficiency is observed to decrease. This negative effect is attributed to increased solution turbidity at higher catalyst concentrations, which causes light scattering and reduces photon penetration to the catalyst surface [18]. Furthermore, excessive catalyst loading can lead to nanoparticle aggregation, which decreases the effective surface area available for the reaction. Therefore, identifying the optimal catalyst dosage is critical for maximizing photocatalytic performance by balancing the availability of active sites with detrimental light-blocking and aggregation effects (Figure 5).

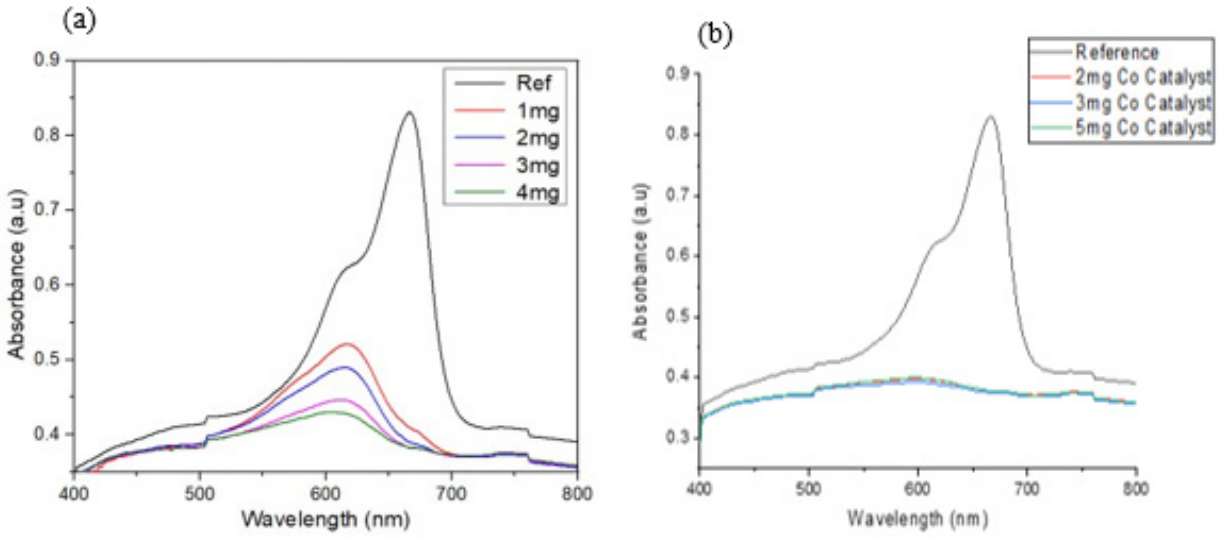

Figure 5: UV-VIS absorption spectra of (a) Ni-doped CeO_2, (b) Co-doped CeO_2 with different concentrations.

A. Effect of initial dye concentration and catalyst stability

The influence of the initial pollutant concentration on the photocatalytic degradation rate was evaluated to understand the reaction kinetics and catalyst efficiency. The photocatalytic activity of the synthesized ceria nanoparticles was tested against Methylene Blue (MB) solutions of varying initial concentrations (10, 20, 30 and 50 ppm) under direct sunlight, using a fixed catalyst dosage of 2mg. The results clearly indicated that the degradation rate is inversely proportional to the initial dye concentration. The most rapid degradation was observed for the 10ppm solution, which achieved complete discoloration in just 10 minutes. This enhanced efficiency at lower concentrations can be attributed to the higher ratio of available active sites on the catalyst surface relative to the number of dye molecules. As the initial dye concentration increases, two primary factors limit the degradation rate: (1) the saturation of the catalyst's active sites, (2) the "inner filter" effect, where the higher concentration of dye molecules in the bulk solution absorbs a significant fraction of the incident light, thereby reducing the number of photons reaching the catalyst surface. This light-shielding effect diminishes the generation of electron-hole pairs, consequently slowing down the overall degradation process.

B. Influence of irradiation source: Direct vs. indirect sunlight

To assess the practical applicability of the synthesized ceria nanoparticles, their photocatalytic activity was compared under both direct and indirect (diffuse) sunlight. This experiment is critical for determining the material's effectiveness in real-world environmental conditions where light intensity can vary. Experiments were conducted using a 10ppm MB solution with a 2mg catalyst dosage and the pH was adjusted to 3, 7, and 11 to re-evaluate the optimal conditions. As anticipated, samples exposed to direct sunlight demonstrated significantly faster and more complete degradation compared to those under indirect light. This is due to the higher photon flux in direct sunlight, which leads to a greater rate of electron-hole pair generation and, subsequently, a higher concentration of reactive oxygen species to degrade the dye. However, it is crucial to note that the catalyst remained active even under indirect sunlight, albeit with a reduced efficiency over the one-hour observation period. This confirms that the material can function under lower-intensity light conditions. Furthermore, these experiments reaffirmed that pH 11 provided the optimal medium for degradation under both direct and indirect irradiation, reinforcing the conclusion that the strong electrostatic attraction between the negatively charged catalyst surface and the cationic

dye in an alkaline environment is a key driver of the reaction's efficiency, regardless of light intensity. These findings underscore the robustness of the catalyst and its potential for application in diverse environmental settings.

C. Effect of pH on particle size distribution of ceria sol

To investigate the influence of synthesis pH on the particle size and colloidal stability of the Ceria sol, Dynamic Light Scattering (DLS) analysis was performed. The DLS data clearly demonstrate a strong correlation between the synthesis pH and the hydrodynamic diameter of the Ceria particles. As shown in Figure 6, the largest average particle size was observed at pH 6, with a peak centred at approximately 1484 nm. As the pH was increased to 8 and 10, the average particle size decreased to 1281nm. A further and more significant reduction was achieved at pH 12, where the particles exhibited the smallest average diameter of approximately 825nm. Notably, the particle size distribution also became narrower as the pH increased. The peak corresponding to the pH 12 sample is visibly sharper and more intense (37.5% of the population) compared to the broader peaks at lower pH values, indicating a more monodisperse and uniform particle suspension under highly alkaline conditions. It is also important to recognize that all measured sizes are in the sub-micron to micron range, indicating the presence of agglomerates rather than discrete primary nanoparticles.

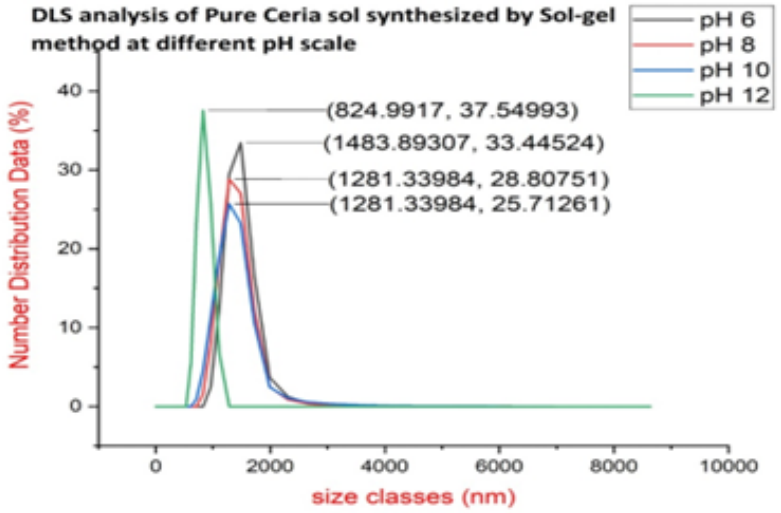

Figure 6: DLS analysis of pure ceria sol synthesized by the Sol-gel method at different pH levels.

D. Proposed mechanism for photodegradation

The positions of the Valence Band (VB) and Conduction Band (CB) can be determined from optical band Gap Energy (EG) values using the following empirical equations [20,21]:

$$E_{VB} = X - E^e + 0.5E_g$$

$$E_{CB} = E_{VB} - E_g$$

In these formulas, EVB and ECB represent the edge potentials of the valence and conduction bands, respectively. X is the semiconductor's electronegativity, calculated as the geometric mean of the electronegativities of its constituent atoms. Ee is a constant representing the energy of free electrons on the hydrogen scale (approximately 4.5 eV). Applying these calculations to the undoped CeO_2 sample, the conduction and valence band edge potentials were found to be -0.67 eV and 2.79 eV, respectively. The introduction of nickel (Ni) or cobalt (Co) ions into the CeO_2 lattice significantly narrows the band gap by creating intermediate energy levels between the original valence and conduction bands. This modified electronic structure is highly advantageous. When the material is exposed to visible light in the Methylene Blue (MB) dye solution, it can absorb light more efficiently than undoped CeO_2. This enhanced absorption leads to the generation of a greater number of electron-hole pairs as electrons are excited from the VB to the CB. Crucially, these dopant energy levels also serve as trapping sites for the photogenerated charges [22,23]. The Ni ion sites preferentially capture electrons, while the Co ion sites act as traps for holes. This strategic separation and localization of charge carriers effectively slow down their recombination rate. By extending the lifetime of the separated electron-hole pairs, Ni and Co doping ensure that more charge carriers can migrate to the catalyst's surface to participate in redox reactions. Once on the surface, the degradation process begins. The cationic MB dye molecules first adsorb onto the catalyst via coulombic attraction to surface hydroxyl (OH-) groups. The trapped holes then react with these OH- ions, while the trapped electrons react with dissolved oxygen. Both pathways lead to the formation of highly reactive hydroxyl radicals (OH). These powerful radicals subsequently attack the functional groups of the adsorbed MB dye, specifically the C-S+=C bond [24], breaking it down into benign final products such as CO_2, SO_4^{2-}, NO_3^-, H_2O, and H+. In summary, this mechanism demonstrates how Ni and Co doping significantly enhances the photocatalytic activity and durability of CeO_2, making the material highly effective for the removal of organic dyes and other pollutants from aqueous solutions.

Conclusions

This work successfully demonstrates that doping cerium oxide (CeO_2) nanoparticles with nickel and cobalt via a sol-gel route is an effective strategy to enhance their photocatalytic activity. Doping was found to systematically reduce both the nanoparticle size and the optical band gap, with the latter enabling more efficient light harvesting. Consequently, all doped catalysts outperformed pure CeO_2 in degrading methylene blue dye under both visible and UV light. The enhanced performance is attributed to improved charge-carrier separation, as dopant sites act as traps that inhibit electron-hole recombination. Notably, both nickel and cobalt yielded the optimal photocatalyst, highlighting its promise for applications in water purification.

CRediT Authorship Contribution Statement

Haider Ali: Conceptualization, Investigation, Writing-original draft. Maqbool Hussain: Writing-review & editing, Fundings. Ghulam Ali: Conceptualization, Writing-review & editing. Shafqat Munir: Writing-review & editing.

CRediT Declaration of Competing Interest

The authors declare that they have no known competing financial interests or personal relationships that could have appeared to influence the work reported in this paper.

References

1. Vasantharaj S, Sathiyavimal S, Saravanan M, Senthilkumar P, Gnanasekaran K, et al. (2019) Synthesis of ecofriendly copper oxide nanoparticles for fabrication over textile fabrics: Characterization of antibacterial activity and dye degradation potential. J Photochem Photobiol B 191: 143-149.
2. Mishra S, Sundaram B (2024) A review of the photocatalysis process used for wastewater treatment. Mater Today Proc 102: 393-409.
3. Goharshadi EK, Samiee S, Nancarrow P (2011) Fabrication of cerium oxide nanoparticles: Characterization and optical properties. J Colloid Interface Sci 356: 473-480.
4. Younis A, Chu D, Li S (2016) Cerium oxide nanostructures and their applications in: Functionalized nanomaterials. In Tech.
5. Murugan R, Vijayaprasath G, Mahalingam T, Ravi G (2016) Defect induced magnetic transition in Co doped CeO_2 sputtered thin films. Ceram Int 42: 11724-11731.
6. Ghosh I, Khamrai J, Savateev A, Shlapakov N, Antonietti M, et al. (1979) Organic semiconductor photocatalyst can bifunctionalize arenes and heteroarenes. Science 365: 360-366.
7. Kumar S, Ojha AK, Ni Co and Ni-Co codoping induced modification in shape, optical band gap and enhanced photocatalytic activity of CeO_2 nanostructures for photodegradation of methylene blue dye under visible light irradiation. RSC Adv 6: 8651-8660.
8. Phokha S, Pinitsoontorn S, Chirawatkul P, Poo-arporn Y, Maensiri S, et al. (2012) Synthesis, characterization and magnetic properties of monodisperse CeO_2 nanospheres prepared by PVP-assisted hydrothermal method, Nanoscale Res Lett 7: 425.
9. Ahmad S, Aadil M, Ejaz SR, Akhtar MU, Noor H, et al. (2022) Sol-gel synthesis of nanostructured $ZnO/SrZnO_2$ with boosted antibacterial and photocatalytic activity. Ceram Int 48: 2394-2405.
10. Channei D, Inceesungvorn B, Wetchakun N, Ukritnukun S, Nattestad A, et al. (2014) Photocatalytic degradation of methyl orange by CeO_2 and Fe-doped CeO_2 films under visible light irradiation. Sci Rep 4: 5757.
11. Sabari Arul N, Mangalaraj D, Pao Chi Chen, Ponpandian N, Meena P, et al. (2012) Enhanced photocatalytic activity of cobalt-doped CeO_2 nanorods. J SolGel Sci Technol 64: 515-523.
12. Hussain M, Ali G, Hussain F, Hussain M, Arif MM, et al. (2025) Silver-doped CeO_2 nanocomposites for photo degradation of selected azo dyes. Journal of the Pakistan Institute of Chemical Engineers 52.
13. Hong Wei He, Xiao Qing Wu, Wei Ren, Peng Shi, Xi Yao, et al. (2012) Synthesis of crystalline cerium dioxide hydrosol by a sol-gel method. Ceram Int 38(Supplement 1): S501-S504.
14. Holzwarth U, Gibson N (2011) The Scherrer equation versus the Debye-Scherrer equation. Nat Nanotechnol 6: 534-534.
15. Joseph C Bear, Paul D McNaughter, Paul Southern, Paul O Brien, Charles W Dunnill (2015) Nickel-doped ceria nanoparticles: The effect of annealing on room temperature ferromagnetism. Crystals (Basel) 5(3): 312-326.
16. Ansari AA, Labis J, Alam M, Ramay SM, Ahmad N, et al. (2016) Effect of cobalt doping on structural, optical and redox properties cerium oxide nanoparticles. Phase Transitions 89(3): 261-272.
17. Muduli S, Ranjan Sahoo T (2023) Green synthesis and characterization of CeO_2 and Ni-doped CeO_2 nanoparticles and its dielectric properties. Mater Today Proc 74(4): 697-702.
18. Murugadoss G, Kumar DD, Kumar MR, Venkatesh N, Sakthivel P, et al. (2021) Silver decorated CeO_2 nanoparticles for rapid photocatalytic degradation of textile rose bengal dye. Sci Rep 11: 1080.
19. Dos Santos ML, Lima RC, Riccardi CS, Tranquilin RL, Bueno PR, et al. (2008) Preparation and characterization of ceria nanospheres by microwave-hydrothermal method. Mater Lett 62(30): 4509-4511.
20. Kumar S, Ojha AK (2015) Oxygen vacancy induced photoluminescence properties and enhanced photocatalytic activity of ferromagnetic ZrO_2 nanostructures on methylene blue dye under ultra-violet radiation. J Alloys Compd 644: 654-662.
21. Feng Guo, Weilong Shi, Xue Lin, Xu Yan, Yu Guo, et al. (2015) Novel $BiVO_4/InVO_4$ heterojunctions: Facile synthesis and efficient visible-light photocatalytic performance for the degradation of rhodamine B. Sep Purif Technol 141: 246-255.
22. Luo M, Liu Y, Hu J, Liu H, Li J, et al. (2012) One-pot synthesis of CdS and Ni-doped CdS hollow spheres with enhanced photocatalytic activity and durability. ACS Appl Mater Interfaces 4(3): 1813-1821.
23. Nishikawa M, Hiura S, Mitani Y, Nosaka Y (2013) Enhanced photocatalytic activity of $BiVO_4$ by co-grafting of metal ions and combining with $CuBi_2O_4$. J Photochem Photobiol A Chem 262: 52-56.
24. A Houas (2001) Photocatalytic degradation pathway of methylene blue in water. Appl Catal B 31: 145-157.